Uncertainty quantification in laser powder bed fusion using multi-physics numerical simulation and copula-based analysis

Zhang, Y.; Nogal Macho, M.; Rocha, I.B.C.M.; Morales Napoles, O.

UNCECOMP 2025
6th ECCOMAS Thematic Conference on
Uncertainty Quantification in Computational Sciences and Engineering
M. Papadrakakis, V. Papadopoulos, G. Stefanou (eds.)
Rhodes Island, Greece, 15–18 June 2025

UNCERTAINTY QUANTIFICATION IN LASER POWDER BED FUSION USING MULTI-PHYSICS NUMERICAL SIMULATION AND COPULA-BASED ANALYSIS

Yunfan Zhang[1], **Maria Nogal**[1], **Iuri B. C. M. Rocha**[1], **Oswaldo Morales-Nápoles**[1]

[1]Faculty of Civil Engineering and Geosciences, Delft University of Technology
Stevinweg 1, 2628 CN Delft, The Netherlands
{Y.Zhang-46, M.Nogal, I.Rocha, O.MoralesNapoles}@tudelft.nl

Keywords: Additive Manufacturing, Powder Bed Fusion, Uncertainty Quantification, Probabilistic Modeling, Copulas, Tail Dependence

Abstract. *Laser powder bed fusion (LPBF), a prominent metal-based additive manufacturing (AM) technique, enables the production of complex, neat-net-shape components with minimal material waste and reduced lead times. However, achieving high final product quality is challenging due to numerous process variables and intricate, nonlinear interactions introduced by LPBF's thermal-mechanical mechanisms. This study employs a copula-based analysis using multi-physics numerical simulations to probabilistically map relationships among process and part quality variables. Dependence and tail-dependence analyses are performed to provide deeper insights into variable interactions, enabling the identification of preferred operational windows with a balanced trade-off between product quality and productivity. The developed methodology advances the understanding of uncertainty propagation in LPBF, contributing toward improved process optimization, repeatability, and reliability.*

1 INTRODUCTION

Additive manufacturing (AM) is a manufacturing technique that builds 3D components by progressively depositing and fusing materials together in a layer-by-layer pattern along a predefined path. In recent years, a type of metal-based AM technique named laser powder bed fusion (LPBF), also known as selective laser melting, has become increasingly popular and broadly applied in various fields, such as the aerospace industry, automotive industry, and medicine. This is mainly attributed to its ability to manufacture neat-net-shape components with highly complicated geometry, minimal material waste, and reduced lead time, in comparison to conventional subtractive manufacturing techniques such as machining and tooling [6].

In any manufacturing process, the primary goal is to produce high-quality components with accurate geometry and reliable mechanical properties. However, in spite of its merits, guaranteeing the repeatability of the LPBF process with satisfied final part quality has been a recurrent research topic. On the one hand, the more sophisticated and dynamic nature of the LPBF process, compared to conventional techniques, introduces additional process variables as sources of uncertainty, making it more challenging to accurately measure and quantify these uncertainties. Furthermore, a complicated multi-physics mechanism is involved in the LPBF process, showing a high-dimensional non-linear relationship between process and part quality variables. Based on these factors, the propagation of uncertainties in process variables and their effect on the variability of part quality variables are highly unpredictable without a systematic analysis method.

In order to address this problem, uncertainty quantification (UQ) techniques have been applied to gain a better understanding of the relationship between process and part quality variables. This is particularly significant in terms of enhancing reliability, guiding robust design decisions, and reducing risk in production. Important efforts have been done in previous works, most of them focus on the (global) sensitivity analysis method either using experimental data or simulation data to directly quantify the variability in part quality variables by varying one or more process variables [17, 13, 18, 19]. In References [16, 12, 21, 2], Bayesian estimation and calibration methods are used to predict the part quality variables in consideration of the associated uncertainties. Some other methods, such as Bayesian networks [9] and genetic programming [8], have been used to perform the UQ analysis. However, most of the existing methods rely on the assumption of simple correlation structures, largely overlooking the possibility of more complex dependencies between variables. Many of these approaches focus on only a small subset of variables, limiting their capacity to capture the full complexity in the multi-parameter LPBF process.

To address these limitations, an analysis method based on copulas is proposed in this work to establish a deeper understanding of the probabilistic relationship among both process variables and part quality variables. Specifically, the strength and structure of the dependencies of the variables are researched in the UQ analysis to identify the key process variables. The tail dependence is evaluated to investigate the possibility of the co-occurrence of extreme values. Based on these analyses, a preferred operational window is suggested to achieve a balance within the trade-off between the final product quality and productivity.

The paper structure is organized as follows: In Section 2, the mechanism of the LPBF process and the relevant process and part quality variables are introduced. In Section 3, the construction of the multi-physics numerical simulation model for the LPBF process and the copula-based analysis are presented. In Section 4, a case study of the Inconel 625 superalloy is introduced,

including the variability for the Monte Carlo (MC) sampling and the configurations for the simulation. In Section 5, the dependence analysis is performed to investigate both the effect of process variables on part quality and the interdependence among the part quality variables themselves.

2 LASER POWDER BED FUSION PROCESS

LPBF is a common type of metal-based AM technique, which manufactures 3D metallic components from material in powder form. In this process, thin layers of metallic powder are deposited on a build platform and selectively fused together by a high-powered laser to build components in a layer-by-layer pattern. This system is mainly composed of three parts: (i) the powder feed system responsible for powder deposition, (ii) the build chamber containing a build platform, powder bed, and inert gas environment, and (iii) the energy delivery system of a laser source. As shown by the process flowchart in Figure 1, the LPBF process starts with a sliced 3D digital model in computer-aided design (CAD). After an optional preheating operation of the build platform, the powder feed system works to evenly deposit a new layer of metallic powder at the top surface of the build platform using a recoater blade. The laser source is navigated through optical control units to scan across the deposed powder layer, melting and fusing the powder together along a pre-defined path of the digital model. Then, the build piston is lowered down, and the operations above are repeated until the last slice of the layer is successfully printed. At the end, the printed component is cooled down and undergoes optional post-processing procedures to improve mechanical properties or surface quality.

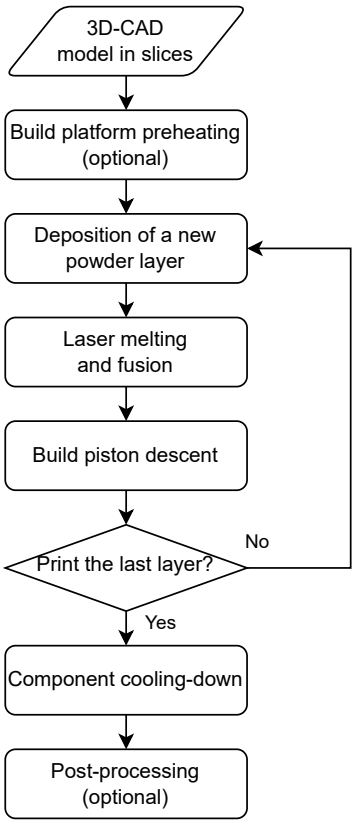

Figure 1: Flowchart of the LPBF process for the manufacturing of a metal component.

The major advantage offered by LPBF is its ability to manufacture near-net-shape components with highly complicated geometry, minimal material waste, and reduced lead times, which is a nearly impossible task for conventional subtractive manufacturing processes. However, the physical process involved in LPBF brings in more complexities. This is mainly reflected in two aspects: (i) The usage of a high-powered laser source and metallic powder feedstock introduces additional process variables as sources of uncertainty, making the accurate quantification of laser and material properties a challenging task. In particular, the powder feedstock is usually more sensitive to the processing environment change due to its loosely distributed state compared to bulk material. Therefore, the variability as well as the change of material properties need to be taken into account before and during the processing cycle. (ii) The LPBF process entails a highly intensive multi-physics mechanism that exhibits a non-linear relationship of high dimensionality between process and part quality variables. This makes a precise prediction of the part quality quite difficult while propagating uncertainty sources through the process model. Therefore, the combined effect of both factors can lead to a final product that does not reach the expected high quality in manufactured components. In order to achieve a stable and reliable LPBF process, a good understanding of the relationship between process variables and part quality variables needs to be established.

There are a large number of process variables that significantly influence the part quality in the LPBF process due to the coexistence of multiple physical models [10]. This work focuses on three types of process variables: variables related to the process itself, the thermal-dependent material properties, and the mechanical material properties. Specifically, these variables are laser power, scan speed, absorptivity, powder density, specific heat capacity, thermal expansion, Young's modulus, and yield stress. The choice of the variables related to the process and thermal properties is primarily based on the existing literature in which dependence has been reported between the melting process and the melt pool evolution [4, 3, 16, 17]. In addition, the mechanical properties are also investigated in this work, as they are playing a crucial role in the formation of distortion and residual strain and stress during the cooling down process. Despite their importance, the effects of thermal expansion, Young's modulus, and yield stress on part quality and the mechanical performance of the final product are largely overlooked in the literature.

After propagating through the non-linear multi-physics model of the LPBF process, the process variables of interest have either a direct or indirect effect on the part quality of manufactured components. To assess the influence of the uncertainty in the process variables, a set representative part quality variables is selected. It consists of the melt pool characteristics during the LPBF process, namely length, height, width, and maximum temperature of the melt pool. These four variables are considered because the melt pool status is one of the most important factors that determines the solidification process, the formation of defects, and consequently, the part quality of manufactured components. For instance, the melt pool with an increased temperature has a weaker surface tension and a smaller dynamic viscosity. This will lead to a recoil effect due to the strong oscillation in melt pool flow and consequently cause the formation of undesirable defects, such as balling, irregularity, distortion, and spatter behind the melt pool track [15]. In addition, other part quality variables that are directly related to the geometric accuracy of manufactured components are also included. The variables are the maximum displacement and maximum residual strain of the solidified material, which are expected to be kept as small as possible. The residual strain here is the L2-normalized equivalent residual strain, which is simply named residual strain in this work for simplicity.

3 METHODOLOGY

To investigate the relationship between process variables and part quality variables, a numerical simulation model is developed to emulate the multi-physics mechanism of the LPBF process in this work. Compared to experimental data, numerical simulation can synthesize an unlimited amount of data without the need for expensive experimental setup and data collection. Moreover, certain part quality variables, such as melt pool dimension and maximum temperature, pose measurement challenges because of the transient manufacturing environment of high temperature. The adoption of numerical simulation enables us to concentrate on the effect of the variability in process variables without the contamination of other sources of uncertainty. In Section 3.1, the mechanism of the multi-physics simulation of the LPBF process is explained.

The synthetic data from the developed model is then analyzed by a copula-based method from a probabilistic perspective. Compared to the sensitivity analysis pattern commonly applied, copulas can capture the complex and joint dependence structures among multiple variables simultaneously, rather than treating each variable's effect in isolation. In addition, copulas can provide more information about the shape and strength of dependence that goes beyond simple correlation measures, offering a deeper understanding of how variables co-vary under different conditions. The theory of the copula and its analysis are introduced in Section 3.2.

3.1 Multi-physics simulation of the LPBF process

The multi-physics simulation model of the LPBF process is constructed based on the work presented in References [20, 11], where the time-dependent thermal-mechanical problem is solved using a one-way coupling approach. In this approach, the solution of the thermal simulation model is taken as the input of the elastoplastic simulation model to solve for the mechanical behavior of the material under the influence of temperature, as illustrated in Figure 2. The simulation assumes isotropic material behavior and perfect plasticity while neglecting factors such as vaporization and powder geometry to focus on the primary thermal and mechanical phenomena.

The thermal simulation shown in Figure 2 is considered a transient heat transfer problem, where the temperature field T_i at any point in the simulation domain is continually changing at each time step i under the effect of external heat energy input. This process is modeled by the heat conduction equation based on Fourier's law in three dimensions

$$\rho C_p \frac{\partial T}{\partial t} = \nabla \cdot (k \nabla T), \tag{1}$$

where T is the temperature distribution as a function of space and time, ρ is the material density, C_p is the specific heat capacity, and k is the thermal conductivity of the heat flux. Notably, the material properties - density, specific heat capacity, and thermal conductivity - are dependent on temperature and typically modeled by linear regression functions to approximate their values in response to temperature.

The elastoplastic simulation shown in Figure 2 is governed by the equilibrium equation in three dimensions, in which the divergence of the stress tensor $\boldsymbol{\sigma}$ must be equal to zero. That is

$$\nabla \cdot \boldsymbol{\sigma} = 0, \tag{2}$$

which assumes there are no body forces in the material.

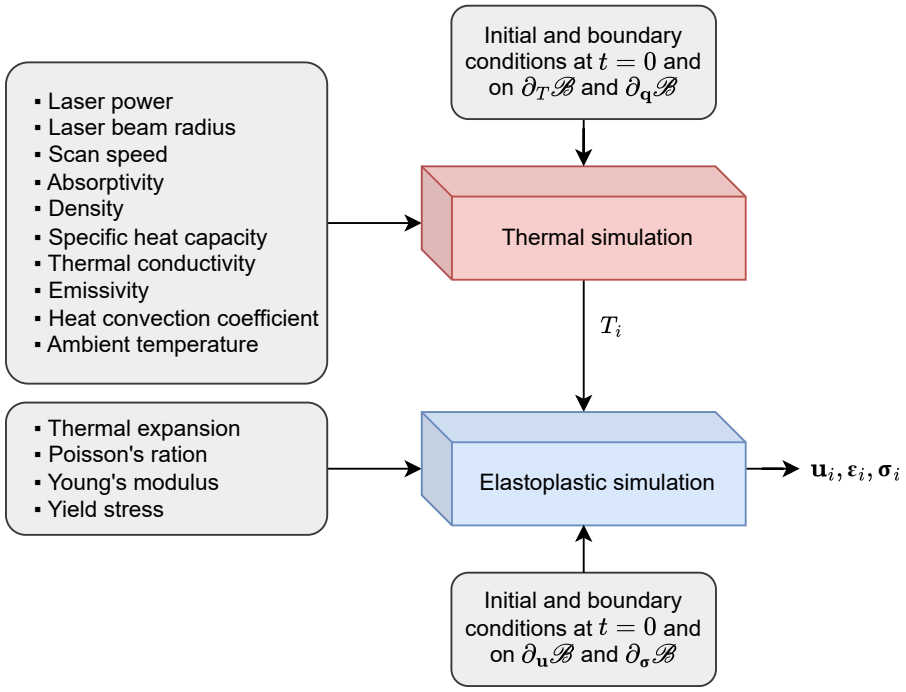

Figure 2: Multi-physics simulation model of the LPBF process using a one-way coupling approach. $(\partial_T \mathcal{B} \cup \partial_{\boldsymbol{q}} \mathcal{B})$ and $(\partial_{\boldsymbol{u}} \mathcal{B} \cup \partial_{\boldsymbol{\sigma}} \mathcal{B})$ are the set of the Dirichlet and Neumann boundaries for the thermal and elastoplastic simulation. T_i, $\boldsymbol{u}_i$, $\boldsymbol{\varepsilon}_i$, and $\boldsymbol{\sigma}_i$ denotes the solution for the temperature, displacement, strain, and stress field at the time step $i = 1, \ldots, n$, respectively.

The constitutive model is defined as J2 perfect plasticity in this case, and the resulting initial boundary value problem (IBVP) is solved using a classic return-mapping algorithm as follows:

$$\begin{aligned} \boldsymbol{\sigma}_{i+1} &= \boldsymbol{\sigma}^{\text{trial}}_{i+1} - \frac{\boldsymbol{s}_{\text{dev}}}{\boldsymbol{s}_{\text{norm}}} \left\langle \boldsymbol{s}_{\text{norm}} - \sigma_y \right\rangle_+ , \\ \boldsymbol{\sigma}^{\text{trial}}_{i+1} &= \boldsymbol{\sigma}_i + \Delta\boldsymbol{\sigma}, \\ \Delta\boldsymbol{\sigma} &= \lambda \text{tr}(\Delta\boldsymbol{\varepsilon}) I + 2\mu \Delta\boldsymbol{\varepsilon}, \end{aligned} \tag{3}$$

where $\boldsymbol{\sigma}^{\text{trial}}$ is the elastic trial stress, $\boldsymbol{s}$ is the deviatoric part of $\boldsymbol{\sigma}^{\text{trial}}$, σ_y is the yield stress, $\boldsymbol{\varepsilon}$ is the strain tensor, and λ and μ are the Lame's parameters. The last term $\left\langle \boldsymbol{s}_{\text{norm}} - \sigma_y \right\rangle_+$ is the yield condition of J2 perfect plasticity, where the operator $\langle \rangle_+$ is defined as a ramp function satisfying $\langle x \rangle_+ = \frac{1}{2}(x + |x|)$. Note that the Lame's parameters are directly derived from the Poisson's ratio ν and the Young's modulus E.

The effect of temperature is taken into account through a thermal strain term $\boldsymbol{\varepsilon}_{\text{th}}$ as follows:

$$\begin{aligned} \Delta\boldsymbol{\varepsilon} &= \boldsymbol{\varepsilon}_{i+1} - \boldsymbol{\varepsilon}_i - \boldsymbol{\varepsilon}_{\text{th}}, \\ \boldsymbol{\varepsilon}_{\text{th}} &= \alpha_V (T_{i+1} - T_i) I, \end{aligned} \tag{4}$$

where α_V is the thermal expansion coefficient. The superscripts in Equations (3) and (4) denote the discretized time step.

As shown in Figure 2, the Dirichlet and Neumann boundary conditions are imposed on both temperature and elastoplastic fields at the set of boundaries $(\partial_T \mathcal{B} \cup \partial_{\boldsymbol{q}} \mathcal{B})$ and $(\partial_{\boldsymbol{u}} \mathcal{B} \cup \partial_{\boldsymbol{\sigma}} \mathcal{B})$,

respectively. Specifically, the heat flux of the laser source q_{laser} is defined at the top surface of the domain and assumed to follow a Gaussian energy distribution as follows:

$$q_{\text{laser}} = \frac{2\eta P}{\pi r_b^2} \exp\left(\frac{-2d^2}{r_b^2}\right), \tag{5}$$

where η is the absorptivity of the material, P is the laser power, r_b is the laser beam radius, and d is the distance between the laser beam center and the material point. Additionally, heat flux terms from convection and radiation are accounted for as described in References [20, 11].

3.2 Copula-based analysis

Copula is a multivariate joint distribution function with uniformly distributed marginals. For a sequence of random variables X_j for $j = 1, \ldots, d$ with a marginal distribution function $F_j(x_j)$, copula is defined by the Sklar's theorem [14] as

$$C(F_1(x_1), ..., F_d(x_d)) = F(x_1, \ldots, x_d), \tag{6}$$

where C is the cumulative distribution function (CDF) of the multivariate copula and F is the joint CDF of the d-dimensional random variables defined on the original scale. In Sklar's theorem, the random variables are standardized by probability integral transform using the marginal distribution function $u_j = F_j(x_j)$, and u_j follows a uniform distribution in the range of $[0, 1]$.

The associated probability density function (PDF) of the multivariate copula can be obtained by calculating its differentiation as

$$c(F_1(x_1), \ldots, F_d(x_d)) = \frac{f(x_1, \ldots, x_d)}{f_1(x_1) \ldots f_d(x_d)}, \tag{7}$$

where c is the copula density and f and f_j are the joint and marginal PDF of the random variables, respectively.

The major advantage offered by the copula lies in its ability to separate the dependence between random variables in spite of the different shapes and ranges of associated marginal distributions. Therefore, it is possible to construct a unique copula for multiple random variables with arbitrary marginal distributions while keeping the dependence structure unchanged. In this work, we primarily focus on bivariate copulas, as they provide a fundamental framework for examining the dependence between two random variables. Numerous families of bivariate copulas - such as Gaussian, Student's t, and various Archimedean types - have been developed. Interested readers are referred to [5] for a detailed overview.

To quantitatively assess the strength of dependence between two random variables, the rank-based correlation coefficient, Kendall's tau τ, is commonly used, which is defined as the probability of concordance minus the probability of discordance of two random variables X_1 and X_2 [5]. Kendall's tau has a range of $[-1, 1]$, with 0 indicating complete independence, 1 for perfect positive correlation, and -1 for perfect negative correlation. Compared to the conventional Pearson correlation coefficient, Kendall's tau is based on the rank and, therefore not dependent on the actual values and ranges of random variables.

In addition to the rank correlation, copula can provide more information with respect to the dependence structure through the tail dependence analysis. The upper and lower tail dependence coefficient of a bivariate copula is defined as

$$\begin{aligned}\lambda^{\text{upper}} &= \lim_{m\to 1^-} P(X_2 > F_2^{-1}(m)|X_1 > F_1^{-1}(m)) = \lim_{m\to 1^-} \frac{1-2m+C(m,m)}{1-m},\\ \lambda^{\text{lower}} &= \lim_{m\to 0^+} P(X_2 \leq F_2^{-1}(m)|X_1 \leq F_1^{-1}(m)) = \lim_{m\to 0^+} \frac{C(m,m)}{m},\end{aligned} \tag{8}$$

where the limiting probability of simultaneous extreme movements in the upper and lower tails are quantified, respectively [5]. The analysis of the tail dependence is of significant importance, particularly for the accurate assessment of extreme risks during manufacturing.

4 APPLICATION CASE

In this work, a numerical simulation focused on single-track scanning is performed to research the thermo-mechanical behavior of the phase-changing material to input process variables in the LPBF process. Specifically, a nickel-based superalloy, Inconel 625, is employed due to the extensive research [20] and industrial experience available on processing this material using AM and LPFB techniques, making it an ideal reference material for the investigation.

An MC simulation is conducted by stochastically sampling the process variables of interest described in Section 2 and using them as inputs to the multi-physics model described in Section 3.1. As a result, the PDFs for the part quality variables are obtained. The mean and standard deviation values for the process variables of Inconel 625 are listed in Table 1. The selection of the mean values is based on previous works and industry standards [1, 19]. A standard deviation of $\pm 10\%$ is assumed to facilitate the analysis of the variables, while the actual variability can be deviated from these values in practical applications. As for the thermal-dependent characteristics modeled by linear regression functions and the values of the constant process variables, we simply adopted the property data from Reference [19] and assumed that the powder material of Inconel 625 shares the same thermal-dependent properties as the bulk material.

Process variable	Units	Mean value	Standard deviation
Laser power, P	W	195	$\pm 10\%$
Scan speed, v_l	mm/s	800	$\pm 10\%$
Density, ρ	kg/m^3	8604	$\pm 10\%$
Specific heat capacity, C_p	J/kg·K	428	$\pm 10\%$
Absorptivity, η	-	0.31	$\pm 10\%$
Thermal expansion coefficient, α	µm/m·K	14	$\pm 10\%$
Young's modulus, E	GPa	150	$\pm 10\%$
Yield stress, σ_y	MPa	650	$\pm 10\%$

Table 1: Mean values and standard deviations of the studied process variables. All the variables are assumed to follow Generalized Beta distributions.

The process variables are assumed to follow Generalized Beta distributions $X_j \sim \text{GBeta}(\alpha, \beta, a, b)$, where X_j denotes the process variable of interest, α and β are the shape parameters, and a and b are the bounds of the support range. The support range is considered as $[0.6\mu_{X_j}, 1.4\mu_{X_j}]$, which corresponds to 4 times the standard deviation from the mean. An advantage of using the Generalized Beta distribution is that the sampled variables are strictly bounded within a support range while keeping a shape resembling a Gaussian distribution, avoiding the sampling of invalid values.

The open-source Python library JAX-FEM [20] is used in this work to construct a numerical simulation model for the LPBF process. The simulation object has a dimension of $3.2 \times 0.8 \times 0.4$ mm^3 in length, width, and depth, with a mesh element size of 20 μm in each direction. The total simulation time is set to three times the laser-on duration, using a time increment of 5 μs. This simulation setting is determined based on a comparison experiment in which various combinations of mesh element sizes and time increments were tested. The combination offering the optimal trade-off between computational time and accuracy was selected. The thermal distribution over the simulation object is computed at every time step, while the mechanical behavior is evaluated every tenth time step in order to reduce computational overhead, as recommended by the library developer [20]. The simulation is run 500 times on TU Delft's supercomputer, DelftBlue [7], producing a sufficient amount of data for further analysis.

5 RESULTS AND DISCUSSION

Based on the MC simulation results, the relationship between (i) each pair of process and part quality variables and (ii) among part quality variables is investigated from a probabilistic perspective. Specifically, a series of bivariate copula functions is fitted for each pair of variables, and the one with the lowest prediction error based on the Akaike information criterion (AIC) is considered the best-fitted copula. Figure 3 shows the rank correlation matrix between the process and part quality variables. Then, the amount and structure of the dependence between the variables are quantified based on the fitted copula and its rank correlation coefficient. Finally, the interaction of the variables in the tail of the fitted copula, that is, the tail dependence, is qualitatively analyzed in terms of its physical implication in the LPBF process.

In Section 5.1, a dependence analysis between the process and part quality variables is performed to investigate the influence of the process variables. In Section 5.2, a dependence analysis solely between the part quality variables is presented to understand how they are correlated to each other and consequently influence the final quality of manufactured components. For the full list of the best-fitted copulas for each pair of the variables, refer to Appendix A.

5.1 Dependence analysis between process and part quality variables

The discussion is structured based on the type of part quality variables involved. Namely, (i) the effect of process variables on melt pool dimension, (ii) maximum temperature, and (iii) maximum displacement and residual strain.

5.1.1 Effect of process variables on melt pool dimension

The stability of the melt pool is one of the most important factors in the LPBF process, as it has a significant impact on the following physical processes, such as microstructure and defect formation, which are directly related to the final quality of manufactured components. Melt pool dimension is a crucial metric to determine the stability of the melt pool development. For instance, a sudden change in the melt pool dimension may imply the occurrence of a mechanical malfunction in operation devices. Moreover, a precise estimation of melt pool dimension in advance can facilitate the optimization of process variables, such as hatch distance and layer thickness, to avoid the occurrence of an unmelted region or porosity due to insufficient or excessive energy input.

Based on the rank correlation coefficient between each process variable and melt pool dimension (last three rows of the matrix shown in Figure 3), laser power and absorptivity are the dominant factors with the largest impact on the length, width, and depth of the melt pool. With

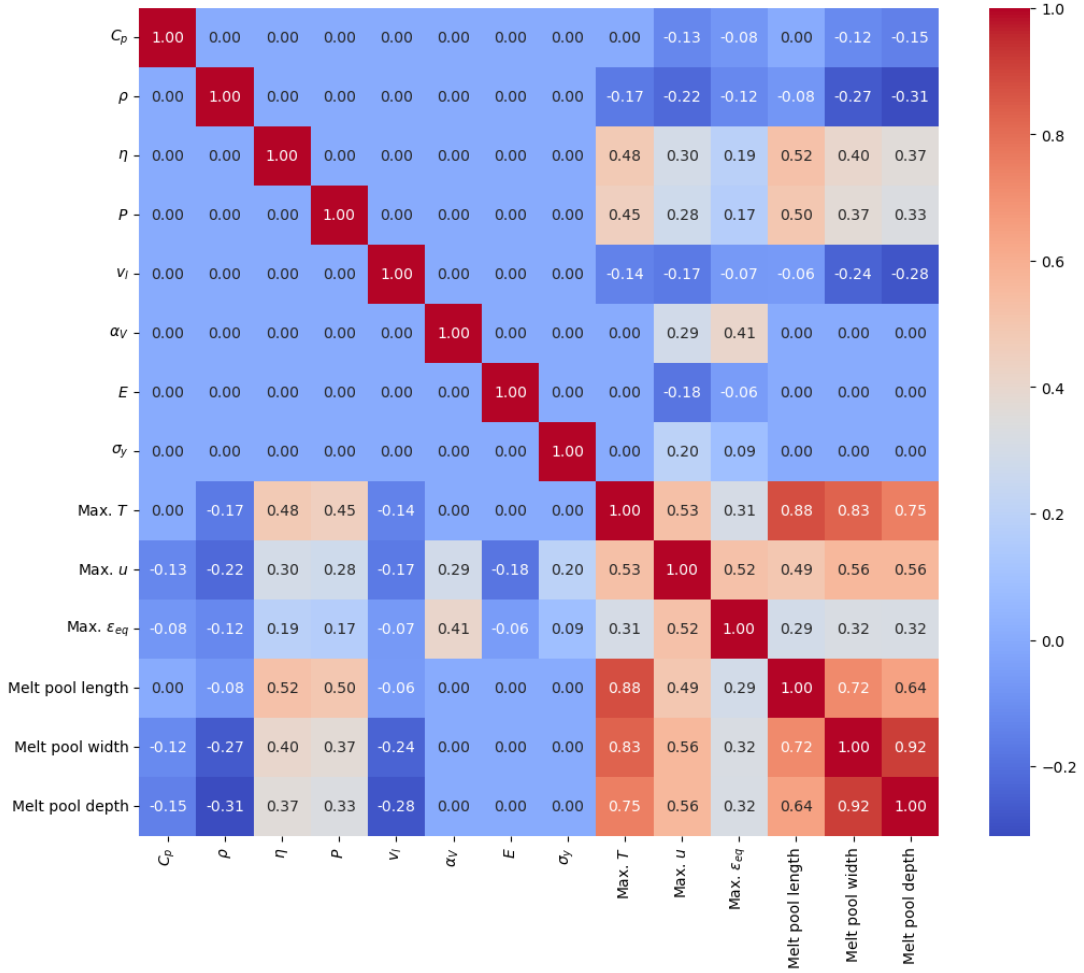

Figure 3: Rank correlation matrix using Kendall's tau between the process and part quality variables and among part quality variables. The rank correlation between process variables to each other is set to 0, as they are sampled from independent GBeta distributions. Most of the variables are defined in Section 2 and 3. u is the magnitude of the displacement and ε_{eq} is the L2-normalized equivalent residual strain.

an increase in absorptivity and laser power, the melt pool size expands correspondingly as a result of a higher energy input. Following that, scan speed, density, and specific heat capacity are less influential, exhibiting a negative correlation to melt pool width and depth. The rest of the process variables (i.e., thermal expansion, Young's modulus, and yield stress) are independent of melt pool dimension. It is noticed that the melt pool length is largely governed by the direct energy input - namely, laser power and absorptivity - while secondary factors such as scan speed, density, and specific heat capacity mostly influence heat conduction in the transverse directions (i.e., width and depth).

The best-fitted copulas for each pair of the process variables and melt pool dimensions are represented in the last three columns of Figure A.3 in Appendix A. It is observed that most of the copulas are Gaussian and elliptically symmetric, and no significant tail dependence is observed. This means that the relationships between the process variables and melt pool dimensions do not exhibit pronounced extreme co-movement at the tails, indicating a consistent correlation structure across the entire data range. The analysis of the tail dependence is of particular importance, as it provides important information about the relationship of associated variables in

extreme conditions to facilitate risk assessment and management.

5.1.2 Effect of process variables on maximum temperature

Similarly, it is observed in Figure 3 that the most influential variables on maximum temperature are laser power and absorptivity, followed by density and scan speed with less impact, and the others are considered independent. This is explained by the heat conduction mechanism introduced in Section 3.1, where more heat energy input, i.e., increased laser power and absorptivity, means a higher maximum temperature and vice versa.

In the first row in Figure A.3, the copulas between the process variables and maximum temperature do not show any tail dependence at both ends, meaning that uniform correlations are maintained across the entire domain.

5.1.3 Effect of process variables on maximum displacement and residual strain

Rows 10 and 11 in Figure 3 show that all the process variables share a similar amount of dependence on maximum displacement with the largest absolute difference of 0.17 between absorptivity and specific heat capacity, whereas only four process variables show evident dependence on maximum residual strain, with thermal expansion as the most dominant factor with a correlation up to 0.41. The process variables that show very low correlations, less than 0.1, are considered independent. Generally speaking, the effect of the process variables on maximum displacement and residual strain demonstrates a similar trend. For instance, an increased heat energy input leads to an increase in both maximum displacement and residual strain. The material that is more sensitive to thermal effects with a greater thermal expansion will accumulate more displacement and residual strain. The main difference is that the residual strain is basically only related to the uncertainties in thermal-dependent properties, while the maximum displacement is influenced by both thermal-dependent and mechanical properties.

By analyzing the tail dependence shown by the best-fitted copulas in the second and third columns of Figure A.3, more information can be extracted in terms of the behavior of maximum displacement and residual strain in extreme conditions. For instance, laser power and absorptivity exhibit a lower tail dependence with respect to maximum displacement. This could potentially be a beneficial property that can be leveraged on purpose to produce geometrically precise components by reducing these process variables by a large margin. On the other hand, the upper tail of laser power, scan speed, and absorptivity is the design space that is expected to avoid as much as possible, as it will lead to a rapid increase in the amount of displacement. The tail dependence of maximum residual strain has a similar but weaker pattern compared to maximum displacement.

Based on the observations above, the synergy effect of both thermal-dependent and mechanical material properties must be delicately considered and designed to control the maximum displacement to a minimum amount. However, there is a trade-off that must be noted in the LPBF process, i.e., the trade-off between final product quality and productivity. Although less heat energy input can produce components with higher accuracy and finer structure, this is usually accompanied by a narrower melt pool and a lower maximum temperature based on the dependent relationships discussed in Section 5.1.1 and 5.1.2, consequently leading to a drop in process stability and productivity.

In addition, materials with a higher Young's modulus and lower yield stress seem to be an appealing choice as they exhibit lower maximum displacement consistently. However, because

the simulation model does not explicitly distinguish between the elastic and plastic strain, the extent of plastic deformation remains unclear. This is potentially detrimental, as a less resilient material is prone to experience more plastic flow rather than staying in an elastic regime, leading to negative impacts on the fatigue behavior of manufactured components. Therefore, further investigation into plastic flow and its response to process parameters is necessary.

5.2 Dependence analysis between part quality variables

Beyond the commonly studied relationship between process and part quality variables, the copula-based analysis allows the investigation of the correlation of part quality variables to each other. This provides an in-depth insight into the LPBF process monitoring from a part quality perspective. In Section 5.2.1, the dependence structure of maximum temperature on other part quality variables is analyzed and discussed. In Section 5.2.2, the focus is mainly on maximum displacement and residual strain. Note that melt pool dimensions are implicitly embedded in the discussion of other part quality variables.

5.2.1 Effect on maximum temperature

In Figure 3, it is observed that the maximum temperature is highly dependent on melt pool dimension (correlation coefficients ranging from 0.75 to 0.88), followed by maximum displacement and residual strain in descending order. This means that an increase in melt pool dimension and maximum displacement and residual strain typically accompanies an increase in maximum temperature, potentially giving rise to unstable melt pool dynamics. In this case, the maximum temperature serves as an effective quality indicator for monitoring melt pool stability in the LPBF process.

By examining the tail dependence structure, we gain further insight into how to maintain a stable operational status with stability in the melt pool dimension and maximum temperature while identifying a preferred operational window with an adequate tradeoff between final product quality and productivity based on qualitative observation. In Figure 4, a strong lower tail dependence is observed between the maximum temperature and other part quality variables, indicating that the part quality variables jointly move toward extreme values. On the other hand, as the part quality variables increase, the maximum temperature exhibits a wider uncertainty range, which poses challenges for process control. Consequently, an operational window close to the lower tail (shown in Figure 4) achieves a favorable balance between final product quality and productivity, providing a reasonable solution for the trade-off problem discussed in 5.1.3. Within this region, the melt pool has a moderate size and is relatively easy to control, while maximum displacement and residual strain remain low.

5.2.2 Effect on maximum displacement and residual strain

In Figure 3, it is observed that maximum displacement and residual strain share a similar pattern of correlation to the part quality variables, with correlation values around 0.50 in the case of maximum displacement and 0.30 in the case of maximum residual strain. The analysis of the part quality variable relationships explains some phenomena that can not be directly derived from their relationship to the process variables. For instance, although the specific heat capacity does not directly affect the maximum temperature, it influences the melt pool dimension through the heat storage and conduction process, which in turn affects the maximum displacement and residual strain.

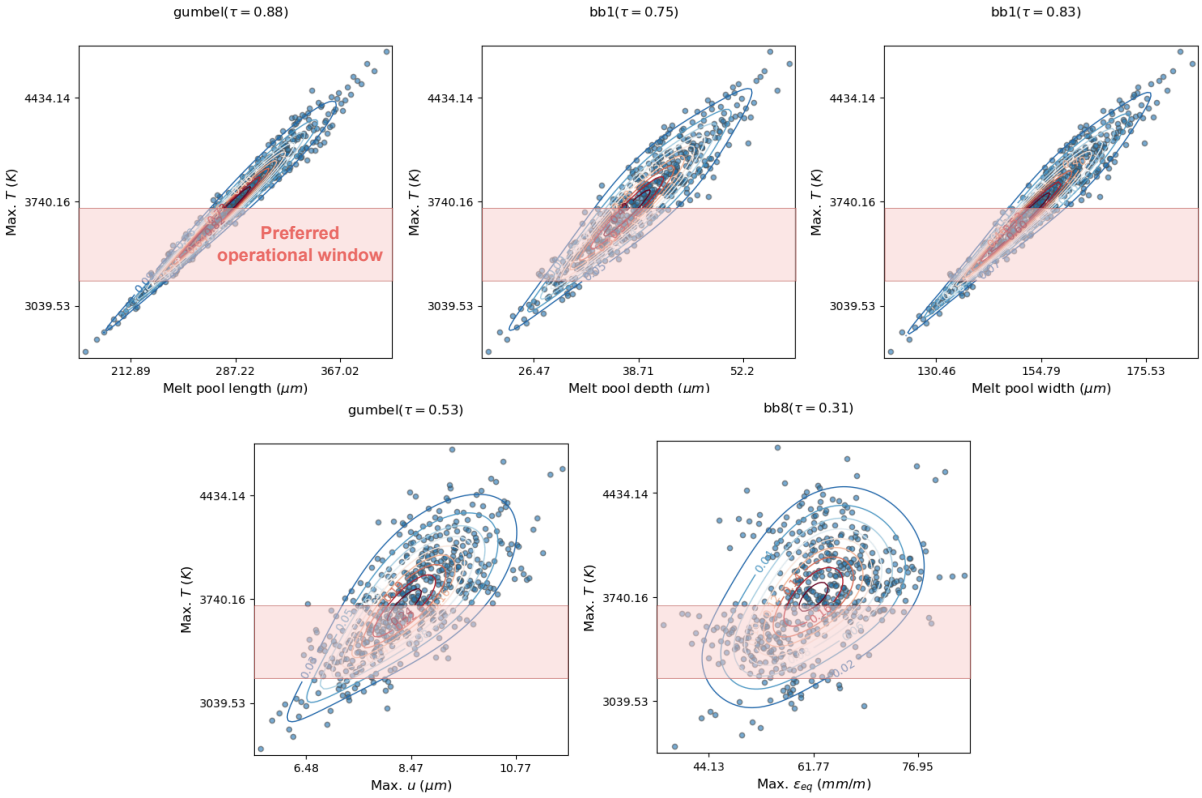

Figure 4: Pair plots of the part quality variables and maximum temperature in a standardized space. The contour curves correspond to the PDF of the best-fitted copula. The type of copula and associated rank correlation coefficient are displayed on the top of the figure. The red box is the preferred operational window that is neither located at the lower tail nor has a large uncertainty range.

The analysis further confirms the existence of the trade-off problem between final product quality and productivity discussed in Section 5.2.2 from a part quality perspective, where a lower degree of distortion is typically accompanied by a narrower and less dynamic melt pool, thus requiring more layers and longer duration for manufacturing the same component. Based on the tail dependence between the part quality variables and maximum displacement and residual strain shown in Figure A.4, it is observed that the pursuit of a very small distortion entails a risk of experiencing a significant drop in melt pool stability. Similar to the analysis procedure discussed in Section 5.2.1, the preferred operational window is located close to the lower tail, as shown in Figure 5, where it is possible to achieve a combination of low distortion but a relatively active melt pool.

6 CONCLUSIONS

In this study, a multi-physics numerical simulation model was used for the LPBF process to enable a UQ analysis of key process variables and their effects on the final product quality. By applying a copula-based approach using simulation data with randomly sampled uncertainties, the nonlinear dependent relationship and tail dependence among both process variables (e.g., laser power, absorptivity, and thermal expansion) and part quality variables (e.g., melt pool dimension, maximum temperature, and maximum displacement and residual strain) are captured. The results revealed that variations in laser power and absorptivity have the most significant impact on the melt pool dimension and maximum temperature, while thermal expansion primarily

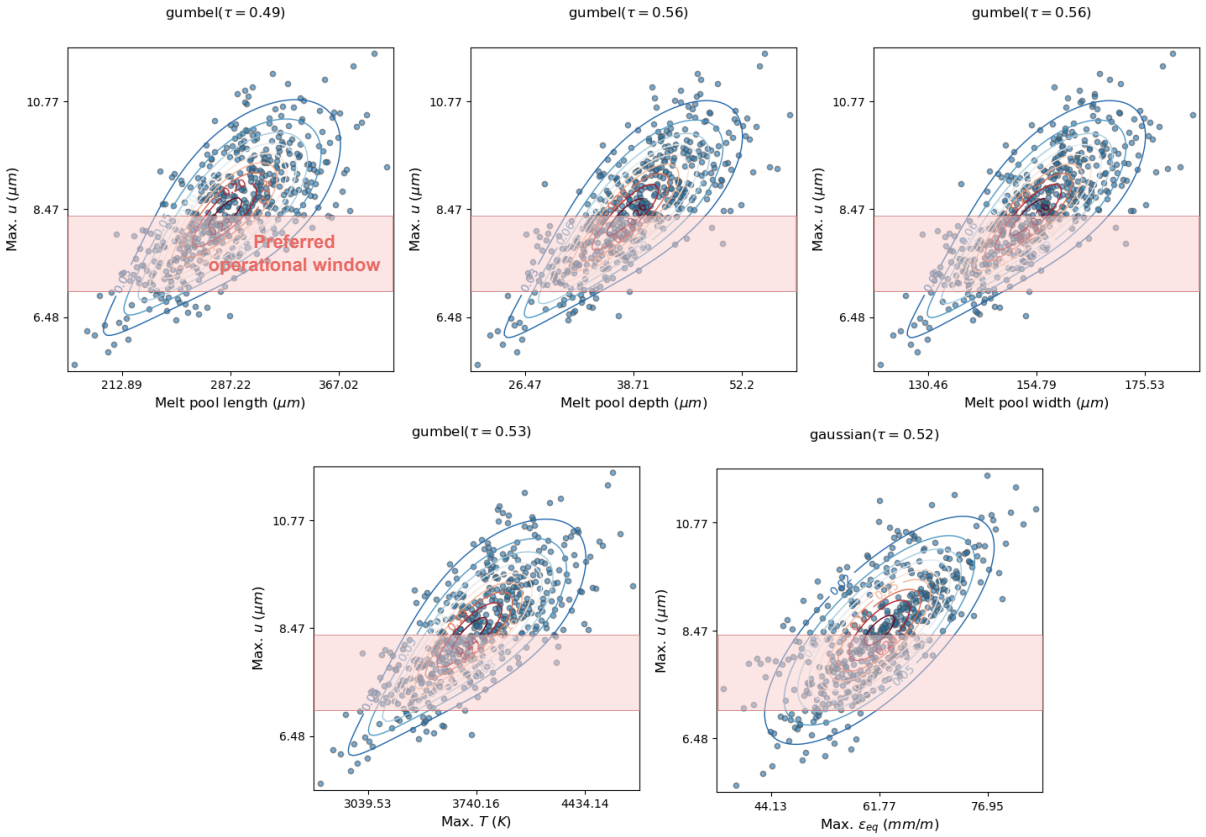

Figure 5: Pair plots of the part quality variables and maximum displacement in a standardized space. The contour curves correspond to the PDF of the best-fitted copula. The type of copula and associated rank correlation coefficient are displayed on the top of the figure. The red box is the preferred operational window that is neither located at the lower tail nor has a large uncertainty range.

drives the variability in maximum residual strain. These findings are in line with previous works [4, 3] and validated from a probabilistic perspective. The maximum displacement is controlled by a synergy effect of both thermal-dependent and mechanical material properties, with each contributing to a similar degree. This is, to our knowledge, the first work to highlight the effect of process variables on maximum displacement. Importantly, tail-dependent relationships support the fact that extreme values in maximum displacement often coincide with extreme thermal or mechanical responses. Based on these analyses, a trade-off problem between the final product quality and productivity was defined in the LPBF process, and a preferred operational window was suggested based on a qualitative observation.

By identifying the dominant process variables that cause significant deviation in part quality from design values, this research advances toward the optimization and control of various parameters in LPBF to enhance repeatability and reliability. For instance, this approach has shown the potential to define operational windows that maximize both the final product quality and productivity. Further efforts are needed in reverse modeling to project these qualitatively observed operational windows back to specific process variables. Together with the relevant physical and technical constraints, the process variable settings that optimize the trade-off between the final product quality and productivity can be determined.

This study has potential limitations, including theoretical assumptions in the numerical simulations, simplified uncertainty ranges that may differ from realistic industrial conditions, and

restriction to bivariate copulas. Future work will address these limitations by incorporating experimental observations through a dependency modeling method of more complexities.

7 ACKNOWLEDGMENTS

We gratefully acknowledge the European Commission for its support of the Marie Sklodowska Curie program through the Horizon Europe DN APRIORI project (GA 101073551).

REFERENCES

[1] Inconel 625. *Wikipedia*, Nov. 2024.

[2] M. Chiappetta, C. Piazzola, L. Tamellini, A. Reali, F. Auricchio, and M. Carraturo. Data-informed uncertainty quantification for laser-based powder bed fusion additive manufacturing. *International Journal for Numerical Methods in Engineering*, 125(17):e7542, 2024.

[3] L. E. Criales, Y. M. Arısoy, B. Lane, S. Moylan, A. Donmez, and T. Özel. Laser powder bed fusion of nickel alloy 625: Experimental investigations of effects of process parameters on melt pool size and shape with spatter analysis. *International Journal of Machine Tools and Manufacture*, 121:22–36, Oct. 2017.

[4] L. E. Criales, Y. M. Arısoy, and T. Özel. Sensitivity analysis of material and process parameters in finite element modeling of selective laser melting of Inconel 625. *The International Journal of Advanced Manufacturing Technology*, 86(9):2653–2666, Oct. 2016.

[5] C. Czado. *Analyzing Dependent Data with Vine Copulas: A Practical Guide With R*, volume 222 of *Lecture Notes in Statistics*. Springer International Publishing, Cham, 2019.

[6] T. DebRoy, H. L. Wei, J. S. Zuback, T. Mukherjee, J. W. Elmer, J. O. Milewski, A. M. Beese, A. Wilson-Heid, A. De, and W. Zhang. Additive manufacturing of metallic components – Process, structure and properties. *Progress in Materials Science*, 92:112–224, Mar. 2018.

[7] Delft High Performance Computing Centre (DHPC). DelftBlue Supercomputer (Phase 2). `https://www.tudelft.nl/dhpc/ark:/44463/DelftBluePhase2`, 2024.

[8] I. Gholaminezhad, H. Assimi, A. Jamali, and D. A. Vajari. Uncertainty quantification and robust modeling of selective laser melting process using stochastic multi-objective approach. *The International Journal of Advanced Manufacturing Technology*, 86(5):1425–1441, Sept. 2016.

[9] N. Hertlein, S. Deshpande, V. Venugopal, M. Kumar, and S. Anand. Prediction of selective laser melting part quality using hybrid Bayesian network. *Additive Manufacturing*, 32:101089, Mar. 2020.

[10] Z. Hu and S. Mahadevan. Uncertainty quantification and management in additive manufacturing: Current status, needs, and opportunities. *The International Journal of Advanced Manufacturing Technology*, 93(5):2855–2874, Nov. 2017.

[11] S. Liao, A. Golgoon, M. Mozaffar, and J. Cao. Efficient GPU-accelerated thermomechanical solver for residual stress prediction in additive manufacturing. *Computational Mechanics*, 71(5):879–893, May 2023.

[12] F. Lopez, P. Witherell, and B. Lane. Identifying Uncertainty in Laser Powder Bed Fusion Additive Manufacturing Models. *Journal of Mechanical Design*, 138(114502), Sept. 2016.

[13] P. Nath, Z. Hu, and S. Mahadevan. Modeling and Uncertainty Quantification of Material Properties in Additive Manufacturing. In *2018 AIAA Non-Deterministic Approaches Conference*, AIAA SciTech Forum. American Institute of Aeronautics and Astronautics, Jan. 2018.

[14] M. Sklar. Fonctions de répartition à N dimensions et leurs marges. *Annales de l'ISUP*, VIII(3):229–231, 1959.

[15] J. Wang, R. Zhu, Y. Liu, and L. Zhang. Understanding melt pool characteristics in laser powder bed fusion: An overview of single- and multi-track melt pools for process optimization. *Advanced Powder Materials*, 2(4):100137, Oct. 2023.

[16] Z. Wang, C. Jiang, P. Liu, W. Yang, Y. Zhao, M. F. Horstemeyer, L.-Q. Chen, Z. Hu, and L. Chen. Uncertainty quantification and reduction in metal additive manufacturing. *npj Computational Materials*, 6(1):1–10, Nov. 2020.

[17] Z. Wang, P. Liu, Y. Ji, S. Mahadevan, M. F. Horstemeyer, Z. Hu, L. Chen, and L.-Q. Chen. Uncertainty Quantification in Metallic Additive Manufacturing Through Physics-Informed Data-Driven Modeling. *JOM*, 71(8):2625–2634, Aug. 2019.

[18] Z. Wang, P. Liu, Y. Xiao, X. Cui, Z. Hu, and L. Chen. A Data-Driven Approach for Process Optimization of Metallic Additive Manufacturing Under Uncertainty. *Journal of Manufacturing Science and Engineering*, 141(081004), June 2019.

[19] S. Wells, A. Plotkowski, and M. J. M. Krane. Propagation of Input Uncertainties in Numerical Simulations of Laser Powder Bed Fusion. *Metallurgical and Materials Transactions B*, 52(5):3016–3031, Oct. 2021.

[20] T. Xue, S. Liao, Z. Gan, C. Park, X. Xie, W. K. Liu, and J. Cao. JAX-FEM: A differentiable GPU-accelerated 3D finite element solver for automatic inverse design and mechanistic data science. *Computer Physics Communications*, 291:108802, Oct. 2023.

[21] J. Ye, M. Mahmoudi, K. Karayagiz, L. Johnson, R. Seede, I. Karaman, R. Arroyave, and A. Elwany. Bayesian Calibration of Multiple Coupled Simulation Models for Metal Additive Manufacturing: A Bayesian Network Approach. *ASCE-ASME J Risk and Uncert in Engrg Sys Part B Mech Engrg*, 8(011111), Oct. 2021.

A FITTED BIVARIATE COPULA FUNCTIONS

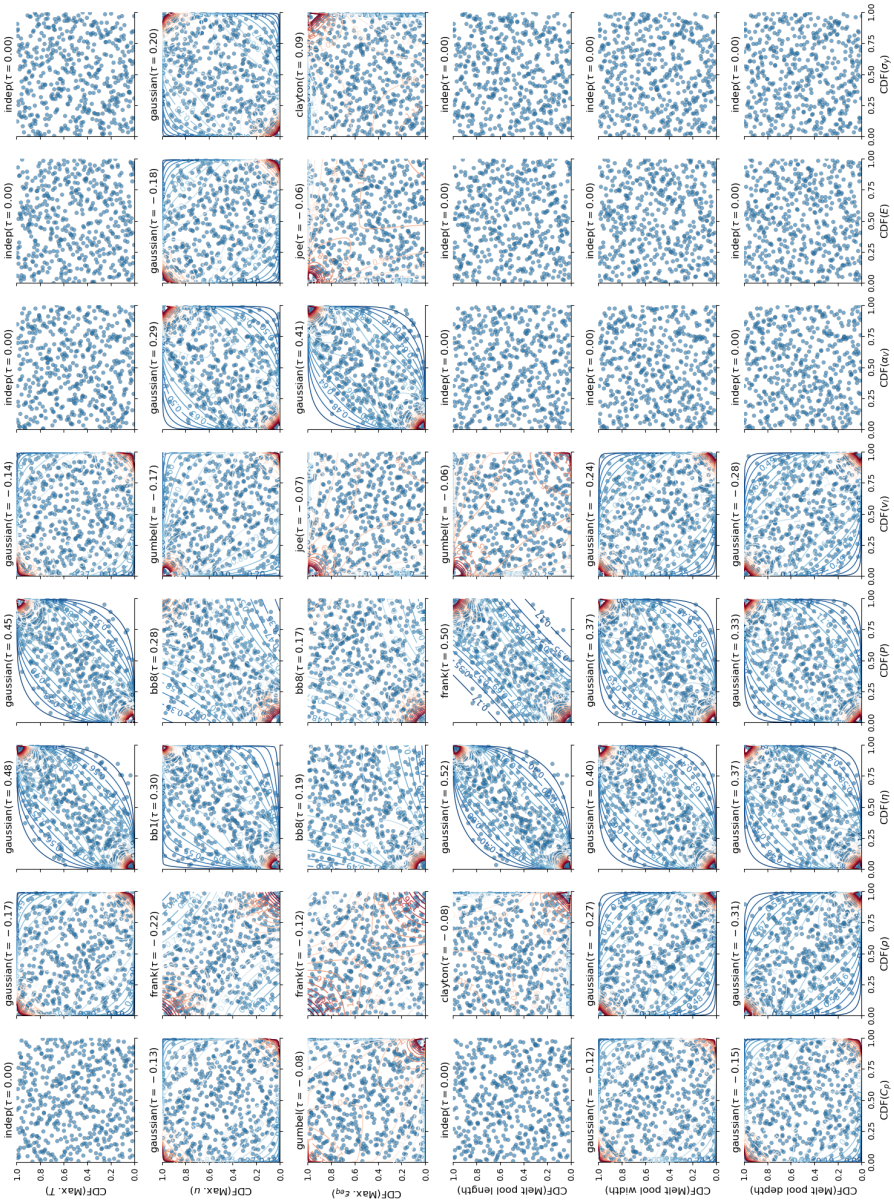

Figure A.1: Pair plots between process and part quality variables, where the contour of the best-fitted copula density function is displayed. Each variable is transformed to uniform space using empirical marginal CDFs. The type and rank correlation coefficient of the best-fitted copula is displayed on the left-hand side of each pair plot.

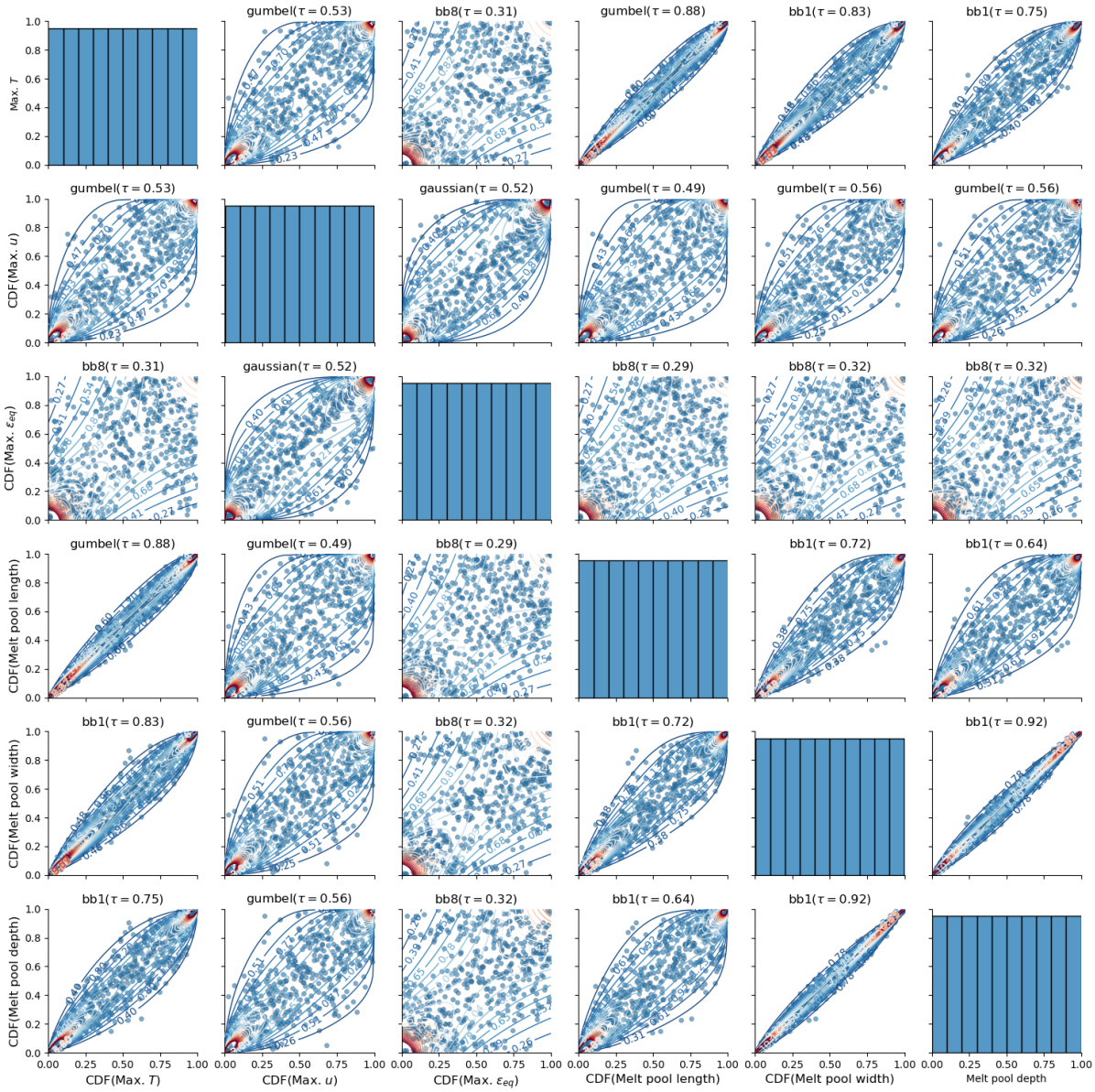

Figure A.2: Pair plots between part quality variables, where the contour of the best-fitted copula density function is displayed. Each variable is transformed to uniform space using empirical marginal CDFs. The type and rank correlation coefficient of the best-fitted copula is displayed on the top of each pair plot. The histogram corresponding to the marginal PDF of each variable is shown in the diagonal.

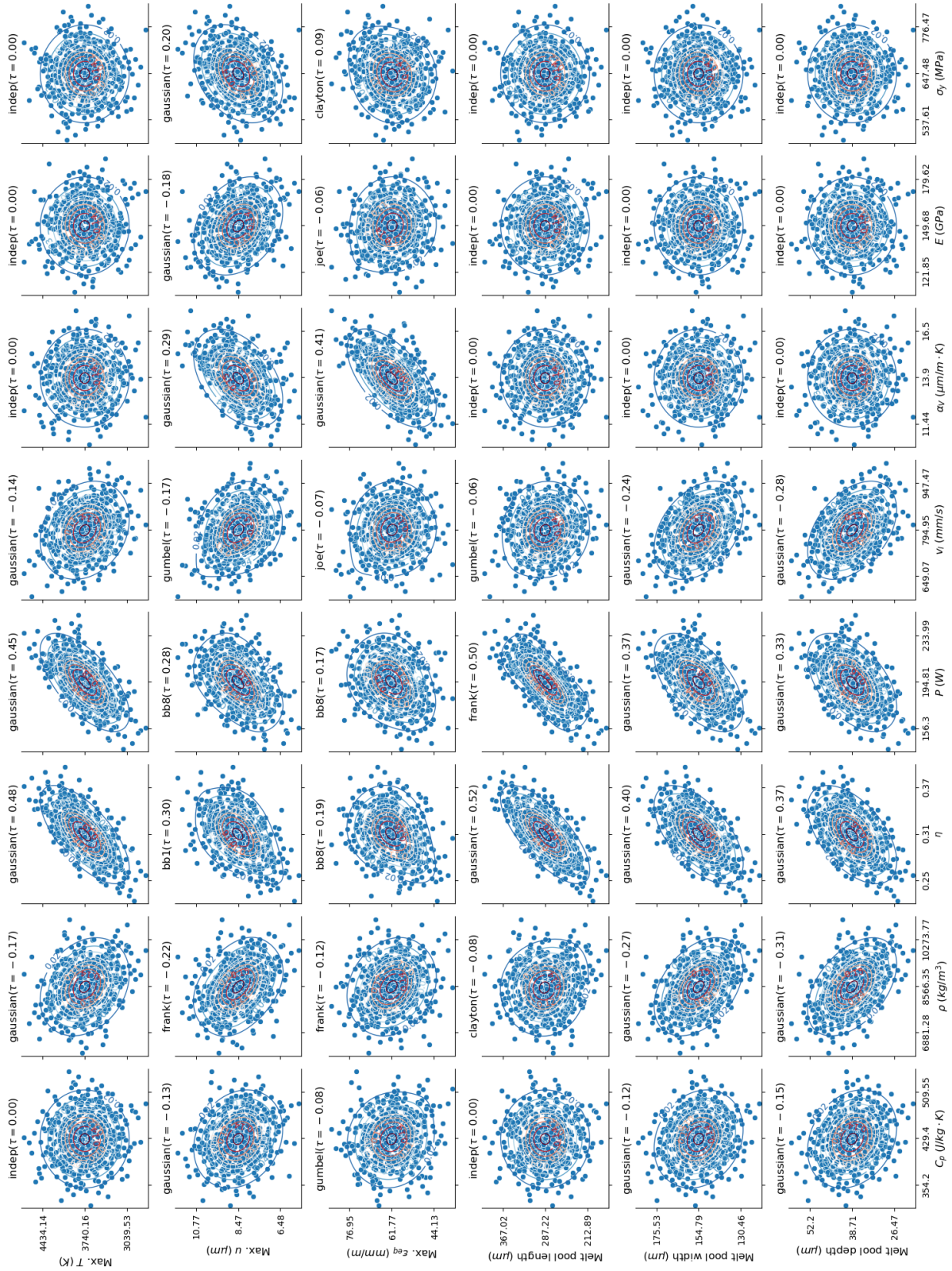

Figure A.3: Pair plots between process and part quality variables, where the contour of the best-fitted copula density function is displayed. Each variable is re-scaled to standardized space by performing inverse univariate Gaussian PDF on the uniform marginal $X_i = \phi^{-1}(u_i)$ and mapped to the original scale. The type and rank correlation coefficient of the best-fitted copula is displayed on the left-hand side of each pair plot.

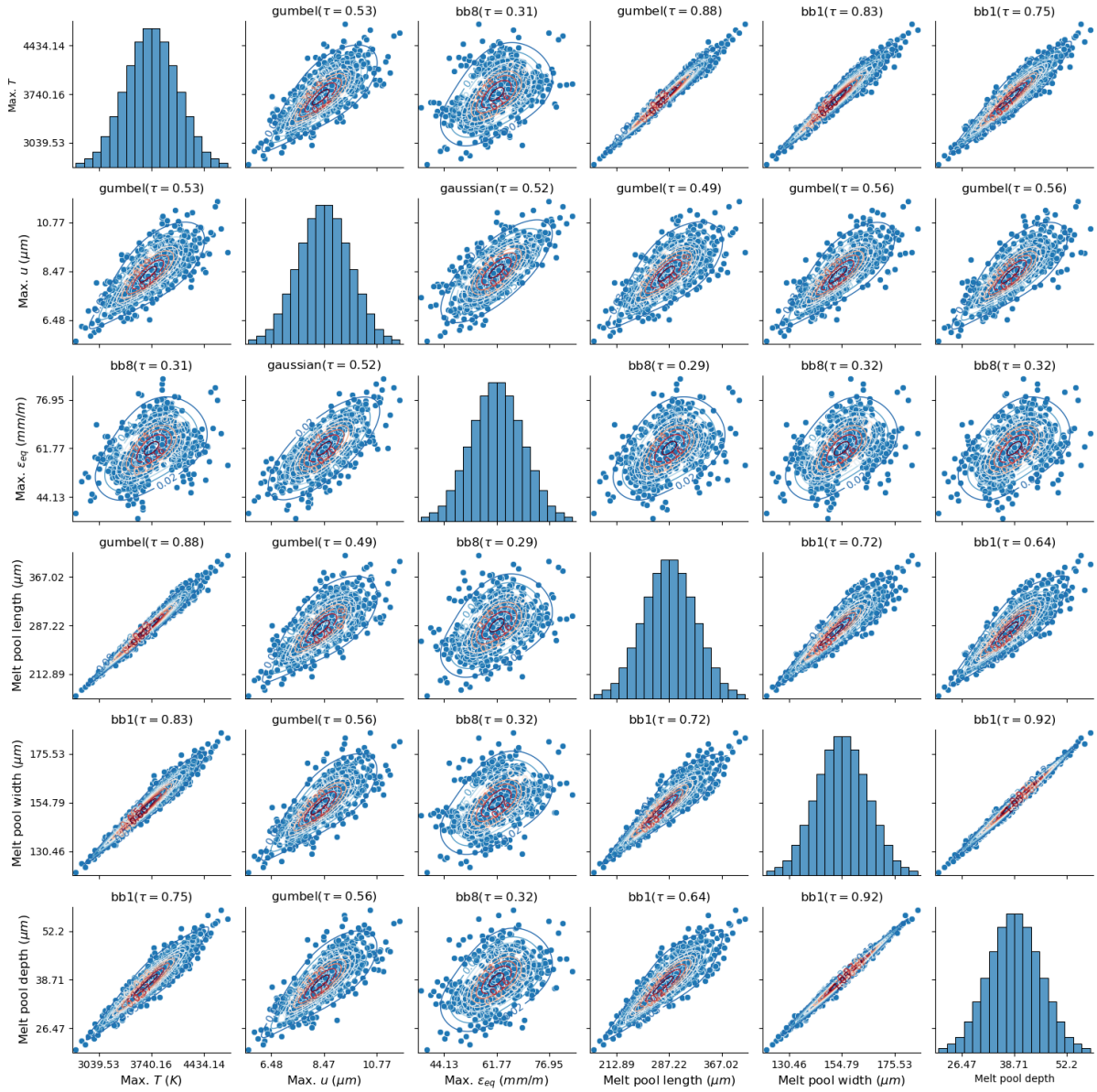

Figure A.4: Pair plots between part quality variables, where the contour of the best-fitted copula density function is displayed. Each variable is re-scaled to standardized space by performing inverse univariate Gaussian PDF on the uniform marginal $X_i = \phi^{-1}(u_i)$ and mapped to the original scale. The type and rank correlation coefficient of the best-fitted copula is displayed on the top of each pair plot. The histogram corresponding to the marginal PDF of each variable is shown in the diagonal.